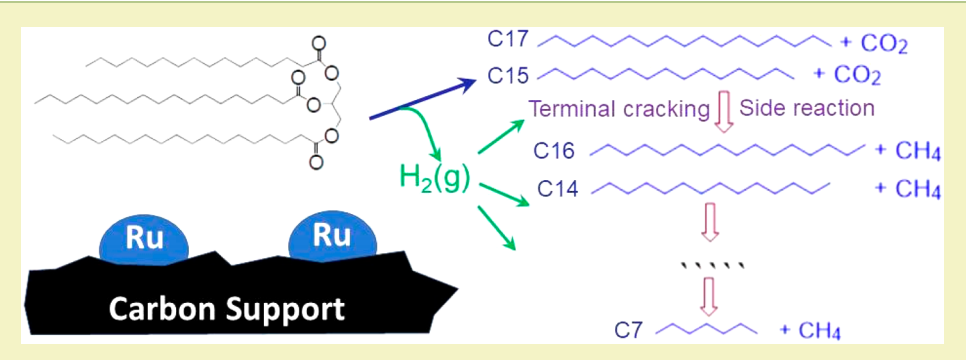


Cite This: ACS Sustainable Chem. Eng. 2019, 7, 14400-14410

Catalytic Hydrothermal Decarboxylation and Cracking of Fatty Acids and Lipids over Ru/C

Jing Zhang,^{†,‡} Xiangchen Huo,[‡] Yalin Li,^{‡,§} and Timothy J. Strathmann*,^{‡,§}

Supporting Information



ABSTRACT: Here, we report on the catalytic hydrothermal conversion of fatty acids and lipids to a range of hydrocarbons using Ru/C without the need for addition of external H2 supplies. Catalyst screening experiments showed the following trend with respect to conversion of stearic acid: Pt/C > Ru/C > Pd/C > Rh/C (nominal 5 wt % metal loadings). Reactions with Ru/ C were then examined further due to its high activity and comparatively low cost. Fatty acid decarboxylation and alkane cracking reactions yield a mixture of liquid n-alkanes of varying chain lengths (mainly as C7-C17) and gaseous products (mainly as CO₂, CH₄, and H₂), with the product distribution dependent on reaction time and initial headspace gas composition. Conversion of an intact lipid (1,2-distearoyl-3-palmitoyl-sn-glycerol) occurs faster than that of stearic acid due to in situ generation of H₂ by aqueous phase reforming of glycerol, a coproduct of the initial triacylglyceride hydrolysis reaction, which, in turn, accelerates fatty acid decarboxylation. Almost complete deactivation of Ru/C was observed after repeated use, but partial recovery of activity was achieved by heat treatment. These findings demonstrate that low-cost Ru catalysts can be applied to produce a mixture of alkanes that can be tailored to match the properties of existing petroleum hydrocarbon fuel blends (e.g., diesel, jet fuel).

KEYWORDS: Green diesel, Hydrocarbon, Jet fuel, Fatty acid, Lipid, Catalyst deactivation

INTRODUCTION

The search for renewable alternatives to petroleum-based fuels has spurred the development of renewable fuels from various sources, including lipid-rich plants and waste materials (e.g., fats, oils, and grease). Recent efforts have shifted away from converting lipid feedstocks to biodiesel (i.e., fatty acid methyl esters, FAMES) in favor of hydrocarbons with a composition similar to petroleum-derived diesel fuel (i.e., so-called "renewable diesel" or "green diesel"). This has most often been accomplished through catalytic hydrodeoxygenation (HDO) of the triacylglyceride structure at elevated temperatures and H₂ pressures (eq 1a-e): 1-5 Green diesel is attractive due to its direct compatibility with petroleum diesel, allowing for full integration with existing refinery and transportation infrastructure.^{6,7} Green diesel production by HDO has been demonstrated for a variety of lipid-rich terrestrial crops (e.g.,

peanuts and soybeans), 8,9 and there is growing interest in applying the process to inedible and waste lipid feedstocks (e.g., waste cooking oil, animal fat, algae lipids, nonedible vegetable oils). Widespread deployment of green diesel production by HDO has been limited by multiple challenges. First, the process exerts a large demand for H2 to reduce the oxygenated functional groups in both the fatty acids and the glycerol coproduct (eq 1b-e). Second, conventional hydrotreatment catalysts (e.g., NiMo and CoMo sulfides) are deactivated by the water produced during HDO reactions.¹⁰ Finally, the alkane hydrocarbons produced by plant-based lipids (typically C₉-C₂₃ alkanes with C₁₈-C₂₃ accounting for

Received: January 12, 2019 Revised: July 18, 2019 Published: August 6, 2019

Key Laboratory of the Three Gorges Reservoir Region's Eco-Environment, Ministry of Education, College of Environment and Ecology, Chongqing University, 83 Shabei Street, Chongqing 400045, People's Republic of China

^{*}Department of Civil and Environmental Engineering, Colorado School of Mines, 1500 Illinois Street, Golden, Colorado 80401, United States

Engineering Research Center for Re-inventing the Nation's Urban Water Infrastructure (ReNUWIt), https://renuwit.org/

$$R_1\text{-COOH} + 3H_2 \xrightarrow{\text{HDO}} R_1\text{-CH}_3 + 2H_2O \tag{1b}$$

$$R_2\text{-COOH} + 3H_2 \xrightarrow{\text{HDO}} R_2\text{-CH}_3 + 2H_2O \tag{1c}$$

$$R_3\text{-COOH} + 3H_2 \xrightarrow{\text{HDO}} R_3\text{-CH}_3 + 2H_2O \tag{1d}$$

$$OH \rightarrow OH + 3H_2 \rightarrow OH + 3H_2O$$
 (1e)

up 25% and aromatics taking up 10%11) have higher molecular weight than petroleum-based fuels, so separate hydrocracking steps may be required to improve fuel characteristics.

To overcome some of the challenges associated with applying HDO, recent efforts have begun to examine hydrothermal catalytic processing as an alternative means of producing green diesel. 7,12–14 Under hydrothermal conditions (e.g., 300–350 °C), 7,12–15 the free fatty acids resulting from hydrolysis of triacylglycerides (eq 1) can be converted to nalkanes via decarboxylation (DOX) reactions (eq 2, left terminal reaction depicted in Figure 1 in place of the HDO pathway, with the former predominating under most conditions). 12,13

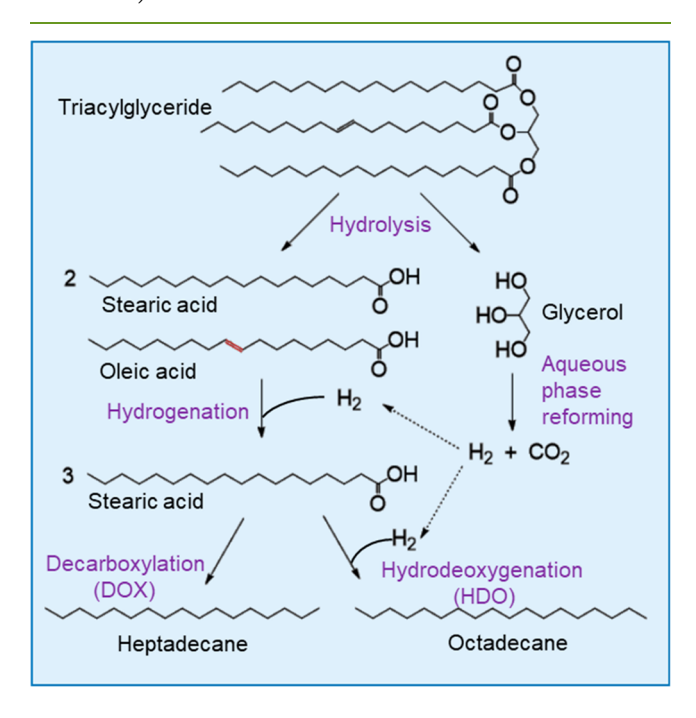


Figure 1. Reaction pathways for catalytic hydrothermal conversion of triacylglycerides to n-alkane hydrocarbons. Adapted from refs 12 and

$$R_1$$
-COOH $\xrightarrow{DOX} R_1$ -H + CO₂ (2)

While HDO reaction products (right terminal reaction depicted in Figure 1) are also observed under elevated H₂ headspace pressures, this is a minor pathway under most hydrothermal conditions.⁷ Predominance of DOX over the HDO reactions is ideal because they require no net consumption of H₂, eliminating the need for external H₂ gas supplies. Furthermore, the limited H₂ requirements for hydrogenating unsaturated fatty acids prior to DOX can often be met through in situ generation of H2 by aqueous phase reforming of the glycerol coproduct of lipid hydrolysis

OH
$$HO$$
 $OH + 3 H2O \rightarrow 7 H₂ + 3 CO₂ (3) Glycerol$

Thus, rather than being a net consumer of H₂, hydrothermal catalytic processing of lipids can be operated as an H2-neutral or even H₂-positive process.^{7,12}

Previous work demonstrates that Pt-based catalysts are effective in promoting both aqueous phase reforming and DOX reactions under hydrothermal conditions, catalyzing the conversion of fatty acids, model triacylglycerides, and a range of waste lipid feedstocks to the corresponding n-alkanes without supplemental addition of H_2 . Although promising, the long-chain *n*-alkane products of many lipid feedstocks require further refining or cracking processes to produce a mixture of hydrocarbons that better reflect the composition of petroleum-derived diesel (carbon numbers ranging from 10 to 15; 75% saturated hydrocarbons, 25% aromatic hydrocarbons)¹⁶ and jet fuels (carbon numbers of 5-16).¹

Here, we report on hydrothermal conversion reactions of fatty acids and lipids using Ru/C as a relatively low-cost alternative to Pt-based catalysts. Initially, a series of carbonsupported noble metal catalysts (Pt/C, Pd/C, Ru/C, and Rh/ C) were screened for their potential to promote conversion of stearic acid in the absence of external H₂ supplies. The results led us to further investigate reactions catalyzed by Ru/C due to its promising activity and low cost relative to other noble metals (Table S1).¹⁸ Feedstock conversions and liquid and gaseous product distributions were measured under wide ranging conditions, and catalyst activity and deactivation were also monitored for several consecutive reaction cycles. Finally, the compatibility of renewable hydrocarbon mixtures produced by Ru/C with petroleum-derived liquid fuels is discussed.

EXPERIMENTAL SECTION

Materials. Stearic acid (98%); glycerol (99.5%); Pt/C, Pd/C, Rh/ C, and Ru/C catalysts (nominal 5 wt % metal content); and C_7 – C_{18} hydrocarbon standards were purchased from Sigma-Aldrich. All the catalysts were used as received. A commercial source of lipid (1,2distearoyl-3-palmitoyl-sn-glycerol) was obtained from City Chemical LLC. Mixed gas standards were obtained from DCG Partnership I, Ltd., USA. ACS-grade dichloromethane and methanol were obtained from Fisher Scientific.

Catalyst Characterization. The bulk metal content of catalysts was analyzed after digestion in KOH-KNO3 by inductively coupled plasma-optical emission spectrometry (ICP-OES; PerkinElmer Optima 2000DV; Galbraith Laboratories). Specific surface areas and pore volumes of the catalysts were determined by N2 physisorption at 77 K (Beckman Coulter SA 3100 adsorption analyzer). Catalysts were degassed at 300 °C in a N₂ atmosphere prior to the analysis. The Brunauer-Emmett-Teller (BET) equation was used to calculate surface areas. Pore volumes were calculated from the desorption isotherms using the Barrett-Joyner-Halenda (BJH) method. Highangle annular dark-field scanning-transmission electron microscopy (HAADF-STEM) images were collected with a JEOL-2100F field emission transmission electron microscope. X-ray photoelectron spectroscopy (XPS) measurements (ESCALAB250, Thermo-VG Scientific) were collected at room temperature under a vacuum of 10^{-8} to 10^{-9} Torr using monochromatic Al Klpha radiation (1486.92 eV). The binding energy (BE) calibration of spectra was accomplished using Au(4f) BE. Metal dispersion was estimated by CO chemisorption using a Micromeritics AutoChem II analyzer equipped with a thermal conductivity detector (TCD). A 1:1 CO/ metal adsorption stoichiometry was assumed. Ru reducibility was determined by H₂ temperature-programmed reduction (TPR) using the same instrument used for CO chemisorption analysis. Samples were first treated with flowing Ar at 20 °C for 60 min to remove any air trapped in the catalyst pores prior to being heated to 800 °C at 10 °C·min⁻¹ in a gas stream of 10% H₂/Ar.

Hydrothermal Conversion Experiments. For a typical batch experiment, water, catalyst, and fatty acid or lipid feedstock were loaded into a Parr 4575 high temperature/pressure reactor (500 mL). The reactor vessel was pressurized at ambient temperature with the desired headspace gas (either N2 or H2) and purged for three cycles before starting the reaction. The headspace pressure was then increased to the desired initial value corrected to 25 °C. Reactor temperature was then raised from room temperature to 330 °C at an average rate of 10 °C min⁻¹ with constant stirring at high speed (>1000 rpm) applied for the desired reaction time. Time zero was set to be the time at which the reaction temperature reached the target value, at which conversions of stearic acid were negligible under 1 MPa nitrogen (0.61%) and hydrogen (1.77%). Once the desired reaction time elapsed, the reactor was rapidly cooled to ambient temperature by initiating water flow through internal cooling coils. For time series studies, independent batch reactions were performed for each time point. After reaction, gas product was collected with a gas sampling bag (Restek) for further analysis. All liquid products and solid catalysts were recovered by extraction with dichloromethane.

In order to check whether the reduction of Ru metal on a Ru/C catalyst would influence its activity, the as-received Ru/C was compared with a catalyst that was pretreated at 300 °C under flowing H₂ for 2 h in a tube furnace. However, no differences in the conversion of stearic acid or formation of products were observed (data not shown). To assess the stability of Ru/C, five successive batch experimental cycles of stearic acid conversion were conducted with the same catalyst batch under 1 MPa N₂ headspace gas (pressure at room temperature before heating reactor). After each run, the liquid sample was collected and extracted with dichloromethane. The Ru/C solids were collected after filtration with a glass fiber filter, washed with dichloromethane, dried at 40 °C, and then reused in the next reaction cycle. Following the fourth run, the dichloromethanewashed catalyst was treated in a tube furnace for 2 h at 300 °C under flowing He before being reused in the fifth reaction cycle. To keep the dosage of Ru/C unchanged during the five consecutive runs, another triplicate set was performed, and the collected catalyst was used to amend any catalyst mass losses during the reuse experiment. All experiments were run in duplicate or triplicate. If two replicates were performed, uncertainty was presented as the full range of values measured surrounding the mean value. If triplicates or more replicates were performed, uncertainty was presented as one standard deviation.

The liquid and gas hydrocarbon products were directly analyzed by gas chromatography (GC, Thermo Fisher Scientific, Trace 1310) with flame ionization detector (FID), with either a HP-5 capillary column (liquid samples) or a Restek Alumina BOND/MAPD column (gas samples). For the liquid products, the injection and detection temperatures were both 250 °C. The column temperature was increased from 100 to 250 °C at a ramp rate of 20 °C min⁻¹. High purity N2 (99.999%) served as the carrier gas. For the analyses of gas products, the injection and detection temperatures were 130 and 200 °C, respectively. The column temperature was kept constant at 135 $^{\circ}\text{C}$ with N_2 as the carrier gas. H_2 CO, and CO_2 gas products were analyzed by a GC (Thermo Fisher, Trace 1310) with a thermal conductivity detector (TCD) and Supelco Carboxen 1010 column. The carrier gases for H₂ and CO/CO₂ were N₂ and He, respectively. The injection and detection temperatures were 100 and 250 °C respectively. The column temperature was increased from 100 to 250 °C at a ramp rate of 25 °C min⁻¹.

The extent of feedstock conversion and molar yields and selectivities of individual products were calculated as mole percentages when stearic acid was used as feedstock (eqs 4-6):

molar yield (mol%) =
$$\frac{\sum n(\text{product})}{n(\text{feedstock})} \times 100\%$$
 (5)

selectivity (mol%)

$$= \frac{n(\text{product})}{n(\text{feedstock before reaction}) - n(\text{feedstock after reaction})} \times 100\%$$
(6)

where n represents the measured number of moles of a particular feedstock or product. Carbon mass balance and carbon mass distribution were calculated using eqs 7 and 8:

$$\left[\sum n(\text{product}) \times \text{carbon number per mole product}\right]$$

$$\left[n(\text{feedstock}) \times \text{carbon number per mole feedstock}\right] \times 100\%$$
carbon mass balance (%) =

carbon mass distribution (%) = [n[product (or feedstock)]]

× carbon number per mole product (or feedstock)]

 $/[n(\text{feed stock}) \times \text{carbon number per mole feedstock}]$ × 100%

(8)

When using the lipid as the feedstock, the measured number of moles of individual products was divided by 3 when calculating molar yields to account for the fact that each triacylglyceride molecule produces three fatty acid molecules during the initial hydrolysis reaction. Initial catalyst turnover frequency (TOF₀) was calculated according to eq

$$TOF_0 = \frac{k_{\text{obs,0}}C_0}{(\text{dispersion} \times C_{\text{catalyst}}W_{\text{metal}})/M}$$
(9)

where $k_{\text{obs},0}$ is the initial observed pseudo-first-order rate constants (h⁻¹) determined by fitting the natural log of fatty acid or lipid concentration versus time data, Co is the initial fatty acid or lipid concentration (mol·L⁻¹), dispersion is estimated from CO chemisorption results, Ccatalyst is the catalyst mass loading in the aqueous suspension (g·L⁻¹), W_{metal} is the Ru mass fraction of the catalyst, and M is the atomic weight of Ru (g·mol⁻¹).

RESULTS AND DISCUSSION

Catalysts Screening. Without any catalyst, no measurable hydrocarbon products were observed with stearic acid [CH₃(CH₂)₁₆COOH] recovery >95%, indicating that hydrothermal processing without a catalyst provides negligible conversion and DOX of stearic acid. Initially, selected Pt group metal catalysts supported on carbon were screened for their activity toward conversion of stearic acid as a representative long-chain saturated fatty acid, under an inert N₂ headspace. Results (Figure 2) showed that activities follow

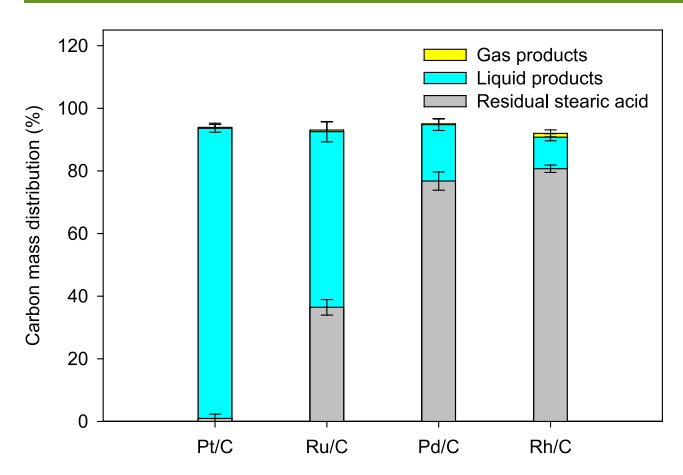


Figure 2. Measured carbon mass distributions from hydrothermal reactions using stearic acid as feedstock under a N_2 headspace with Pt/C, Ru/C, Pd/C, and Rh/C. The gas products include CO_2 and C_1 – C_5 alkanes, while the liquid products include C_7 – C_{18} alkanes. Reaction conditions: 5 g stearic acid, 0.5 g catalyst, 80 g H₂O, initial headspace gas = 1 MPa N_2 at room temperature, preset reaction temperature 330 °C, reaction time = 5 h.

the order of Pt/C > Ru/C > Pd/C > Rh/C. The high activity observed for Pt/C is consistent with earlier reports. 12, Appreciable hydrothermal conversion of stearic acid (roughly 60%) to liquid alkane products was also achieved with Ru/C after reaction for 5 h. In comparison, little conversion was observed with either Pd/C or Rh/C (application of the carbon support itself only resulted in <4% of DOX of stearic acid, indicating the contribution from carbon support was minor, Figure S1). Snare et al. reported a better performance for stearic acid DOX when using Pd/C, Pt/C, and Rh/C compared to Ru/C (Pd > Pt > Rh > Ru). 19 However, their study was performed in an organic solvent (dodecane), while research presented here was carried out in aqueous solution. Fu et al. also observed a lower efficiency of Pd/C than of Pt/C for the catalytic hydrothermal DOX of palmitic acid, 13 consistent with our observations. Thus, the reaction media might significantly influence the performance of an individual catalyst. Relatively high conversion of stearic acid was observed with both Pt/C and Ru/C, but the observed products differed significantly. Conversion and DOX of stearic acid with Pt/C yielded stoichiometric amounts of a single product, heptadecane, similar to an earlier report on Pt reactions with a series of saturated fatty acids. 12 In contrast, a stearic acid reaction with Ru/C yielded a mixture of shorter-chain alkanes in addition to heptadecane, demonstrating the importance of additional reaction pathways.

Even though the observed activity of Ru/C was lower than that of Pt/C, its lower price ¹⁸ (Table S1) suggests a potentially viable alternative that could lower hydrothermal processing costs. The performance of Ru/Al₂O₃ during catalytic hydrothermal processing of stearic acid was also evaluated, and comparable activity was observed for Ru/Al₂O₃ and Ru/C (Figure S1), further demonstrating that Ru is the major active species responsible for the DOX of stearic acid. As a result, further experiments were undertaken to characterize the mechanisms of Ru/C reactions with fatty acids and lipids under hydrothermal reaction conditions, identify factors influencing reaction kinetics, and assess catalyst stability and deactivation.

Ru/C-Catalyzed Reaction of Stearic Acid. Complete conversion of stearic acid to alkanes over Ru/C was observed within 12.5 h under 1 MPa N₂ headspace gas (Figure 3). The initial rate of stearic acid conversion corresponds to an initial catalyst turnover frequency $(TOF_0) = 17.5 \pm 1.4 \ h^{-1}$. On a carbon mass basis, liquid alkanes (C_7-C_{17}) accounted for most of the products observed (>90%), with smaller amounts of gas products (C_1-C_5) alkanes (C_7-C_1) . Figure 3b shows the range of n-alkane products observed at different reaction times.

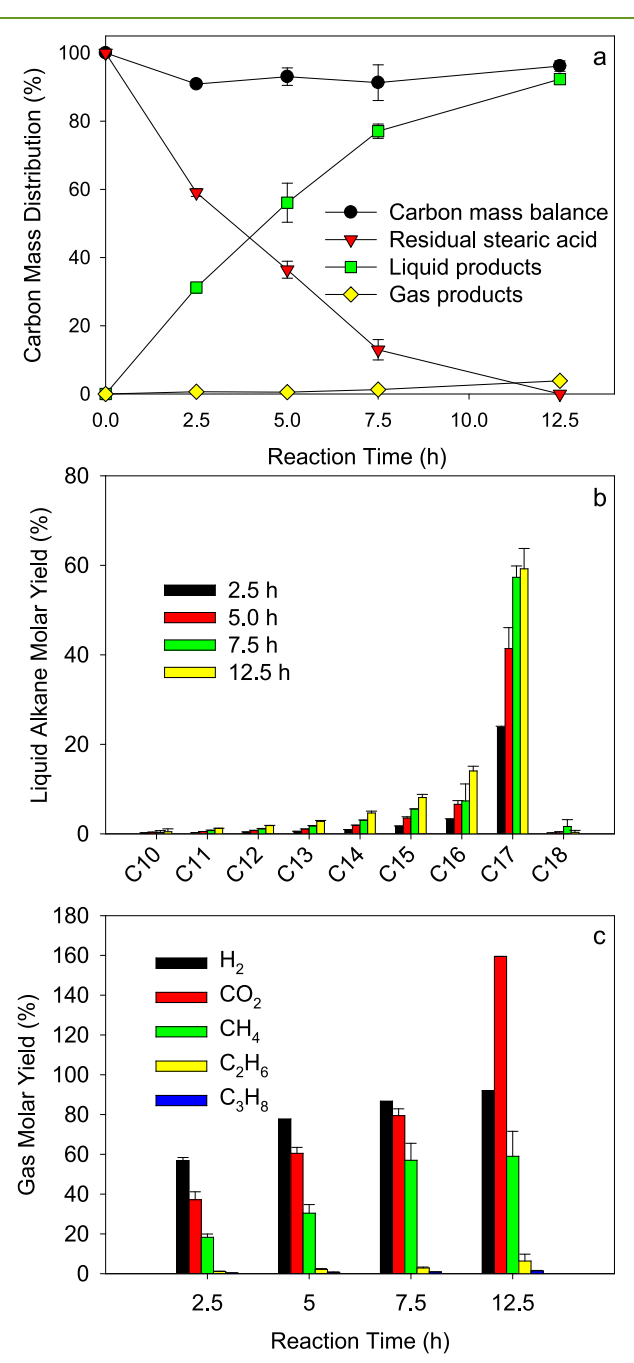


Figure 3. (a) Time course for hydrothermal conversion of stearic acid under N_2 headspace with Ru/C and molar yield ditributions of (b) liquid and (c) gas products (mol %, $n(\text{product})/n(\text{stearic acid}) \times 100\%$). $C_{10}-C_{18}$ labels refer to n-alkane products with 10 to 18 carbon atoms. Reaction conditions are the same as Figure 2. The 160% molar yield of CO_2 indicates there are additional sources for the production of CO_2 other than DOX.

While n-heptadecane (C_{17}) was the product with greatest yield, small amounts of C₁₈ (n-octadecane) product following the HDO pathway were also observed. More importantly, the yield of alkanes gradually decreased with carbon number declining from 17 to 10. Compared with a single alkane product observed for Pt/C, the mixture of alkanes observed with Ru/C may, in fact, be favorable given that existing petroleum-derived diesel and jet fuels are mixtures of hydrocarbons. Petroleum diesel contains hydrocarbons with carbon atoms in the range of 10-15,16 and jet fuel contains hydrocarbons with 8-16 (kerosene type) and 5-15 (widecut/naptha-type) carbon atoms. 17

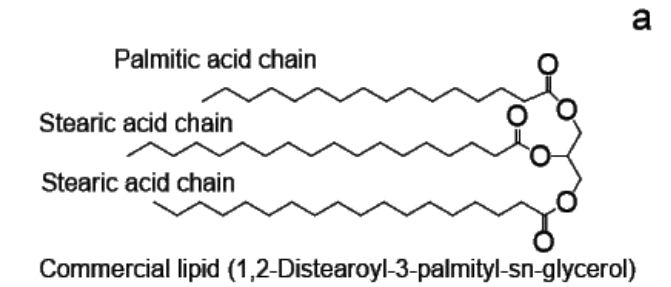
There are two plausible pathways for formation of the shorter chain alkane products: (1) stearic acid first cracks to form shorter chain fatty acids, by losing one or more carbon atoms, which then undergo DOX to form the corresponding *n*alkanes, 20 or (2) stearic acid first undergoes DOX to form an n-heptadecane $(C_{17})^{7,12,13,15}$ which subsequently cracks to form the shorter chain alkanes observed. No shorter chain fatty acids with a carbon number <18 were detected during reactions, leading to a conclusion that DOX was the initial reaction step. N-heptadecane (C_{17}) can then undergo sequential cracking to form shorter-chain alkanes by cleaving a terminal methyl group to form a C_{n-1} alkane and methane. Significant quantities of methane were observed with increasing reaction time (Figure 3c), consistent with earlier reports that Ru/C is an active and selective catalyst for CH₄ formation in supercritical water gasification processes.^{21,22} In addition, we confirmed the cracking of n-heptadecane (C_{17}) by Ru/C in separate experiments where n-heptadecane (C_{17}) was added to the reactor as the initial feedstock with no stearic acid present (Figure S2). Finally, sequential DOX followed by cracking was supported by the observed product selectivities (Figure S3), where selectivities to n-heptadecane (C_{17}) and noctadecane (C_{18}) reached a peak value after 7.5 h (65.8 \pm 0.4% and $1.9 \pm 1.1\%$, respectively) before decreasing at 12.5 h (59.2 \pm 3.2% and 0.3 \pm 0.3%, respectively). These findings contrast with those reported by Miao et al. for reaction with a Ni/ZrO₂ catalyst,²⁰ where shorter chain fatty acid intermediates were observed. Both the metallic Ni and the ZrO₂ support have a very different property from the Ru and carbon support used in this study, which may have distinct effects on the selectivity to different products. Direct (noncatalytic) thermal cracking of stearic acid was reported by Hossain et al., 23 but we observed no measurable heptadecane or other lighter alkane products in the control experiment without any catalyst, indicating the lighter alkane products in the presence of Ru/C are mainly from the cracking of heptadecane instead of stearic acid.

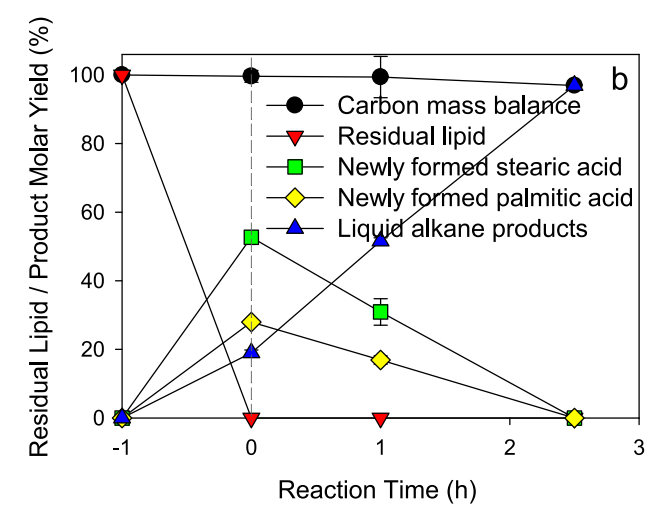
In addition to methane (CH₄), major gas products included carbon dioxide (CO₂) and hydrogen (H₂), with much smaller amounts of ethane (C_2H_6) and propane (C_3H_8) ; Figure 3c). CO2 is a byproduct of fatty acid DOX reactions wherein the terminal carboxylate group is cleaved (Figure 1). However, the molar yield of CO₂ (mol %, $n(CO_2)/n(\text{stearic acid}) \times 100$) exceeded 100% of the initial stearic acid molar concentration, indicating that there were additional sources of CO2 other than the DOX reaction. This was confirmed by comparing the molar yields of CO_2 (mol %, $n(product)/n(feedstock) \times 100$) measured during hydrothermal reactions of heptadecane (29.7%) versus stearic acid (60.5 \pm 2.1%) after 5 h of reaction at 330 °C under 1 MPa N₂ headspace. Thus, the hydrothermal reaction of alkane hydrocarbons with water and/or the reforming of alkane itself at high temperature and high

pressure can substantially affect the end products. Very little carbon monoxide (CO) was detected, indicating that either little CO was generated or that any CO formed was rapidly consumed in water-gas shift and/or methanation reactions.²⁴ The in situ generation of H2 during hydrothermal reactions of stearic acid was observed with a molar yield (mol %, $n(H_2)$ / $n(\text{stearic acid}) \times 100\%)$ gradually increasing from 56.7 \pm 1.2% at 2.5 h to 92% at 12.5 h, consistent with previous reports using PtSn_x/C²⁵ and Pt²⁶ as catalysts. H₂ formation can occur via the reforming of alkanes and fatty acids in the presence of $H_2O.^{20}$ As already mentioned, the observed formation of CH_4 is consistent with the cracking of longer chain alkanes by sequential cleavage of terminal methyl groups, as will be discussed in section Enhanced DOX and Cracking under H2.

Finally, the influence of headspace pressure was examined. For most reactions conducted here, the reactor headspace was initially pressurized with 1 MPa N₂ before heating the reactor to the set point temperature (330 °C). Under these conditions, complete conversion of stearic acid occurred after ~12.5 h. Increasing the initial N₂ headspace pressure accelerated the conversion process, reducing the time for full conversion to \sim 5 h with 2 MPa N_2 (TOF₀ = 26.3 \pm 3.1 h⁻¹) and ~2 h with 5 MPa N₂ (TOF₀ = 65.7 \pm 4.7 h⁻¹; Figure S4). It is unclear how the elevated N2 pressure is acting to enhance reaction kinetics since it is an inert gas that does not directly participate in the DOX and cracking reactions. A similar phenomenon was reported by Bhattacharjee and Tan, 27 where enhanced rates of DOX and alkane production were observed with Fe/SBA-15 when headspace pressure with CO2 and N2 was increased. The pressurized inert gas is believed to reduce viscosity and thus reduce the diffusion resistance and increase rates of mass transfer. ^{28–30} Also, the solubility of reacting gases, for example H₂, is enhanced in solvents containing a pressurized inert gas. 28-30 As a result, more dissolved H₂ is available to bind to the surface of the catalyst nanoparticles, which would also cause an increase in the reaction rate.²⁷

Ru/C-Catalyzed Conversion of Lipid. Experiments were also carried out using a commercial lipid feedstock (1,2distearoyl-3-palmityl-sn-glycerol). Since the elevated N₂ headspace pressure from 1 to 5 MPa largely enhanced DOX of stearic acid and cracking of alkanes, the reaction rate of lipid conversion under 5 MPa N₂ might be too high for us to record the changes of reactant (lipid), intermediates (fatty acids), and products (alkanes) during the whole reaction, which may prevent an accurate comparison of lipid results with those of stearic acid. Thus, an intermediate headspace pressure of 2 MPa was chosen in this section. As shown in Figure 4, the lipid hydrolyzed completely during the reactor heat up period (~1 h), with the formation (molar yield) of $52.7 \pm 0.2\%$ stearic acid, 28.0 \pm 0.5% palmitic acid, and 19.0 \pm 0.6% liquid alkanes. The relative quantities of stearic and palmitic acid were consistent with the stated composition of the parent lipid (two stearic acid chains and one palmitic acid chain). The overall rate of H₂ formation was significantly accelerated in comparison to the reaction of stearic acid under the same conditions. All the fatty acids were then converted to hydrocarbons within 2.5 h under 2 MPa N2 headspace pressure, compared with 5 h to achieve the same level of conversion when stearic acid was used as the feedstock (Figure S4). The increased kinetics are attributed to in situ formation of H₂ by aqueous phase reforming of the glycerol coproduct that formed during the initial hydrolysis reaction step (eq 3).





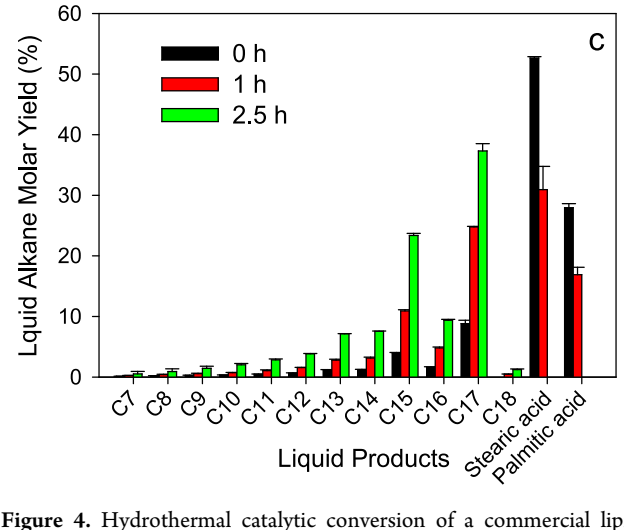


Figure 4. Hydrothermal catalytic conversion of a commercial lipid with Ru/C under $\rm N_2$ headspace. (a) Structure of lipid feedstock, 1,2-distearoyl-3-palmityl-sn-glycerol (containing two stearic acid chains and one palmitic acid chain). (b) Time course for hydrolysis and DOX and (c) liquid product molar yields. Reaction conditions: 5.05 g of commercial lipid (5.9 mmol, wherein the molar ratio of fatty acids in this lipid equals that of 5 g of stearic acid), 0.5 g of catalyst, 80 g of $\rm H_2O$, initial headspace gas = 2 MPa $\rm N_2$ at room temperature, preset reaction temperature 330 °C.

Previous reports with Pt-based catalysts demonstrate that amending reactors with H_2 accelerated DOX of saturated fatty acids. Here, the headspace concentrations of H_2 measured in Ru/C reactions initiated with the lipid (18.6 \pm 0.1 mmol) were nearly double the concentration measured in reactions initiated with stearic acid (9.8 \pm 0.2 mmol) under the same conditions. Similar enhancement of stearic acid DOX under H_2 headspace was also confirmed for Ru/C (Figure 5a), where stearic acid

conversion was complete within 1 h under 1 MPa H₂ (compared to 12.5 h under 1 MPa N₂), corresponding to a $TOF_0 = 131.5 \text{ h}^{-1}$. Furthermore, stearic acid conversion by Ru/C and in situ H₂ generation were similarly enhanced under a N₂ atmosphere when glycerol was added to the reactor (Figure S5). Stearic acid was only partially decarboxylated (37.4% conversion) to alkanes within 1 h when no glycerol was added, and analysis of the reactor headspace gas revealed moderate quantities of H_2 formation (9.8 \pm 0.2 mmol, Table 1). When glycerol was added to the reactor, both the conversion of stearic acid (90% in 1 h) and the yield of H₂ $(22.7 \pm 0.5 \text{ mmol})$ increased considerably, while glycerol was completely consumed (Figure S6). The production of H₂ in the glycerol-only reaction was comparable to those reactions where stearic acid was also present, confirming that hydrothermal DOX of fatty acids is not a H₂-consuming process, consistent with previous reports. Finally, the conversion of stearic acid amended with glycerol was comparable to that observed for the reaction where headspace is pressurized with H₂ (95.6%; Figure S5), confirming that the increase in H₂ pressure was likely the reason for the accelerated DOX reaction observed.

Enhanced DOX and Cracking under H₂. As discussed above, Ru/C-catalyzed DOX reactions of stearic acid were markedly enhanced under H₂ headspace (Figure 5a) even though H_2 does not directly participate in the DOX reaction (eq 2). Vardon et al. attributed the enhanced DOX reactions with Pt-Re/C under H₂ to the presence of the reducing gas acting to maintain the catalyst active metal sites in their reduced oxidation states. In addition to enhancing DOX rates, the subsequent alkane cracking reactions were increased by the elevated H₂ pressure, where the production of liquid alkane reached a peak at 1 h before dropping off with increasing reaction time (Figure 5a,b). At the same time, increasing yields of alkane gas products and ${\rm CO_2}$ were observed (Figure 5a and c), consistent with previous reports.³¹ Furthermore, whereas a small net consumption of H₂ was observed over the first 1 h when DOX reactions predominated, H₂ consumption increased considerably at later reaction times when cracking reactions predominated (Figure 5c). The growth in H₂ consumption almost exactly mirrored the production of methane (inset in Figure 5c), suggesting that the cracking of alkanes was the major pathway responsible for H₂ consumption (eq 10):³²

$$CH_3 - (CH_2)_{15} - CH_3 + H_2 \rightarrow CH_3 - (CH_2)_{14} - CH_3$$

+ $CH_4 \rightarrow CH_3 - (CH_2)_{15-n} - CH_3 + nCH_4 (0 \le n \le 15)$ (10)

The small drop in the mass balance observed after 0.5 h is attributed to experimental artifacts associated with recovering insoluble stearic acid from the reactor by dichloromethane extraction. Vardon et al. reported a net consumption of H_2 during hydrothermal reactions of oleic acid and glycerol with Pt–Re/C carried out under an elevated initial pressure of $H_2 > 3.4$ MPa, where stearic alcohol and octadecane products were observed. The additional H_2 consumption was attributed to olefin hydrogenation reactions and HDO reactions of the terminal carboxylic acid group. No stearic alcohol and only trace C18 alkane (molar yield of 1.45% after 1 h reaction) were observed in the present study, so the enhanced C–C cracking reactions (eq 10) are presumed to be responsible for most of

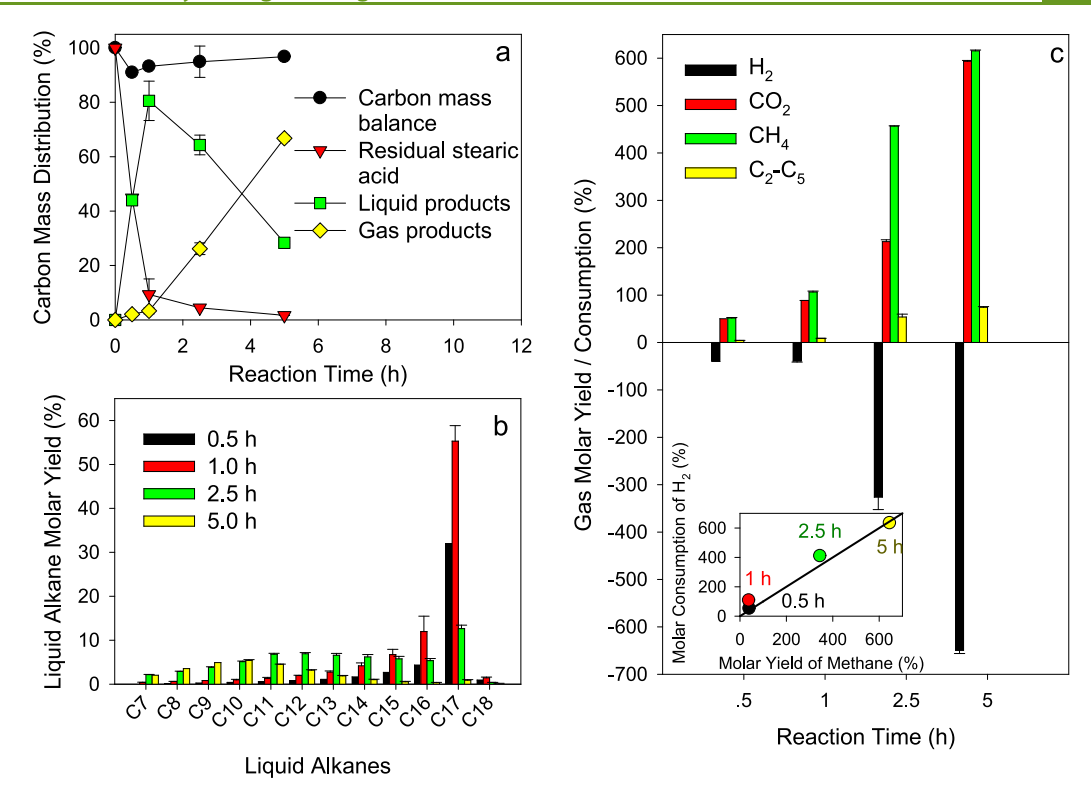


Figure 5. Effect of initial H_2 head gas on stearic acid conversion with Ru/C: (a) reaction time course, (b) liquid product molar yield distribution at different reaction times, and (c) production or consumption of headspace gases at different reaction times. The inset in c shows the linear correlation between molar consumption of H_2 and the molar yield of methane from 1 to 5 h. C_2-C_5 in c refers to alkanes with carbon numbers ranging from 2 to 5. Reaction conditions: initial headspace gas = 1 MPa H_2 at room temperature, and other conditions are the same as in Figure 2.

Table 1. In Situ H_2 Production, Fatty Acid Conversion, and Alkane Molar Yield after Reaction for 1 h Using Ru/C with an Initial Gas Headspace Pressure of 2 MPa

initial headspacegas	feedstock (mmol)	glycerol loading (mmol)	in situ produced H_2 in headspace (mmol)	fatty acid conversion (%)	carbon distribution in gas (%)	liquid alkanes molar yield (%)
N_2	stearic acid (17.6)	0	9.8 ± 0.2	37.5 ± 1.9	3.4 ± 0.5	31.4 ± 1.7
N_2	commercial lipid ^a (5.9)	0	18.6 ± 0.1	55.8 ± 3.2	7.7 ± 0.1	50.9 ± 1.3
N_2	stearic acid (17.6)	5.9	22.7 ± 0.5	89.1 ± 1.6	24.7 ± 0.5	66.0 ± 0.9
H_2	stearic acid (17.6)	0	-308 ± 2.9^{b}	95.6 ± 1.2	41.6 ± 0.3	67.3 ± 1.0
N_2		5.9	21.1 ± 2.5		100	

^aCommercial lipid contains 5.9 mmol glycerol + 17.7 mmol of ester-bonded fatty acids (11.8 mmol stearic acid + 5.9 mmol palmitic acid). ^bNegative value indicates net consumption of H₂.

the $\rm H_2$ consumption observed during reactions performed with an initial $\rm H_2$ head gas. These findings are consistent with the documented reactions using Ru as a catalyst for gasification reactions involving cleavage of C–C bonds that yield $\rm CH_4$, $\rm CO_2$, $\rm H_2$, and $\rm CO$.

Under H_2 headspace gas, the liquid alkane selectivity increased from 79.8% at 0.5 h to 88.8 \pm 1.7% at 1 h before decreasing to 28.8 \pm 0.3% after 5 h (Figure S7). Selectivities to n-heptadecane (C_{17}) and n-hexadecane (C_{16}) displayed similar trends. The highest selectivity to C_{11} – C_{15} was observed at 2.5 h, while that for C_7 – C_{10} was not reached until 5 h. These observations are consistent with the continuous cracking of alkanes to CH_4 and CO_2 with extended reaction time (Figure Sc). Treusch et al. also reported that greater cracking occurred due to a longer residence time in the HDO of liquid phase pyrolysis oil over a sulfided $CoMo/Al_2O_3$ catalyst. In brief, the Ru/C-catalyzed cracking of alkanes is highly sensitive to H_2 pressure. At lower H_2 pressure, little cracking occurs and H_2 consumption is minimal, whereas at high H_2 pressure, cracking

rates increase significantly and net H_2 consumption is observed. It follows that the final mixture of alkane products can be controlled by monitoring and carefully modulating the H_2 pressure in the reactor, which offers a strategy to match the characteristics of green diesel with petroleum-derived diesel and jet fuels.

Stability and Deactivation of Ru/C. Catalyst stability and recyclability is critical for both economic and environmental sustainability of biomass conversion processes. Therefore, we conducted a series of batch experiments to provide an initial assessment of the stability and recyclability of Ru/C during hydrothermal conversion of fatty acids. A single batch of Ru/C was recycled for five consecutive batch reactions to convert stearic acid to hydrocarbons. Partial conversion conditions (7.5 h reaction time) were selected to enable more accurate quantification of deactivation. Results presented in Figure 6 show a gradual deactivation of Ru/C with respect to the DOX of stearic acid, wherein the extent of stearic acid conversion decreased from $86.5 \pm 2.6\%$ in the first cycle to

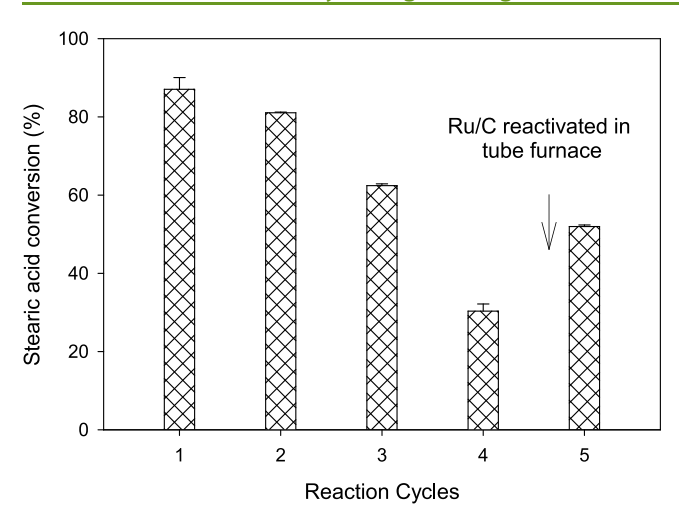


Figure 6. Stearic acid conversion in repeated hydrothermal reaction cycles using the same batch of Ru/C. Reaction conditions for each reaction cycle: 5 g of stearic acid, 0.5 g of catalyst, 80 g of H_2O , initial headspace gas = 1 MPa N_2 at room temperature, preset reaction temperature 330 °C, reaction time = 7.5 h.

 $30.3 \pm 1.3\%$ in the fourth cycle. Prior to the fifth cycle, the Ru/C was treated in a tube furnace for 2 h under a He flow at 300 °C, which partially restored its activity with stearic acid conversion increasing to $52.0 \pm 0.3\%$ in the fifth run.

Analysis of the fresh and used catalyst (after the fourth reaction cycle) showed pronounced reductions in Ru loading, specific surface area, and pore volume. Ru loading was reduced from 3.9 wt % in the fresh catalyst to 2.0 wt % after four runs with trace Ru detected in the aqueous solution (28, 12, 15, and 9 μ g L⁻¹ after the first, second, third, and fourth run, respectively). The BET surface area dropped from 735.3 m² g⁻¹ to 38.9 m² g⁻¹, and average pore volume decreased from 0.64 cm³ g⁻¹ to 0.49 cm³ g⁻¹. The average pore diameter increased from 3.8 to 14.7 nm. Collectively, these findings

indicated a collapsed support structure²⁶ or catalyst fouling. For example, the micropores in the support might be blocked by feedstock,³⁷ identified reaction products,³⁷ or coking deposits. 26,38 Ping et al. stated that after organic extraction to remove the surface-deposited organic reactants and products, a nearly complete recovery of total surface area, pore volume, and active palladium surface area was achieved for a deactivated mesoporous silica-supported palladium nanoparticle catalyst used in the DOX of fatty acids.³⁷ Thus, in our study, the spent Ru/C (after fourth run) was washed with dichloromethane and heated under flowing He at 300 °C for 2 h to remove the organic deposit on the catalyst. Trace condensable white solid was observed at the two ends of tube furnace after treatment, which was presumed to be unreacted stearic acid or hydrocarbon products.³⁷ Partial recovery in activity was observed, which may result from the partial removal of the surface-deposited organic species, i.e., feedstock, or products. A future study on the regeneration of the catalyst is needed to recover its activity and clarify the reasons for catalyst deactivation, especially in continuous-flow reactors (e.g., catalyst packed bed) over extended reaction times.

HAADF-STEM images show that the size distribution of Ru particles in the fresh Ru/C (2.3 ± 0.4 nm, Figure 7a) is statistically different from that measured after the fourth reaction cycle (4.3 ± 1.6 nm, Figure 7b). This indicates the hydrothermal reaction also promotes sintering of the immobilized Ru nanoparticles, which is confirmed by the significant decrease of the metal dispersion on the activated carbon support (Table 2). Fu et al. 12 and Vardon et al. 2 also reported the sintering of Pt nanoparticles in Pt/C and Pt–Re/C after the hydrothermal process, respectively. The sintering of Ru nanoparticles may also lead to the deactivation of Ru/C. 37

 $\rm H_2$ TPR analysis probed the oxidation state of Ru in the fresh and deactivated catalyst. The position of peaks in the mass-normalized TPR profiles (Figure S8) of fresh Ru/C and its counterpart after the fourth reaction cycle are similar, but the intensities for different peaks are obviously different, with

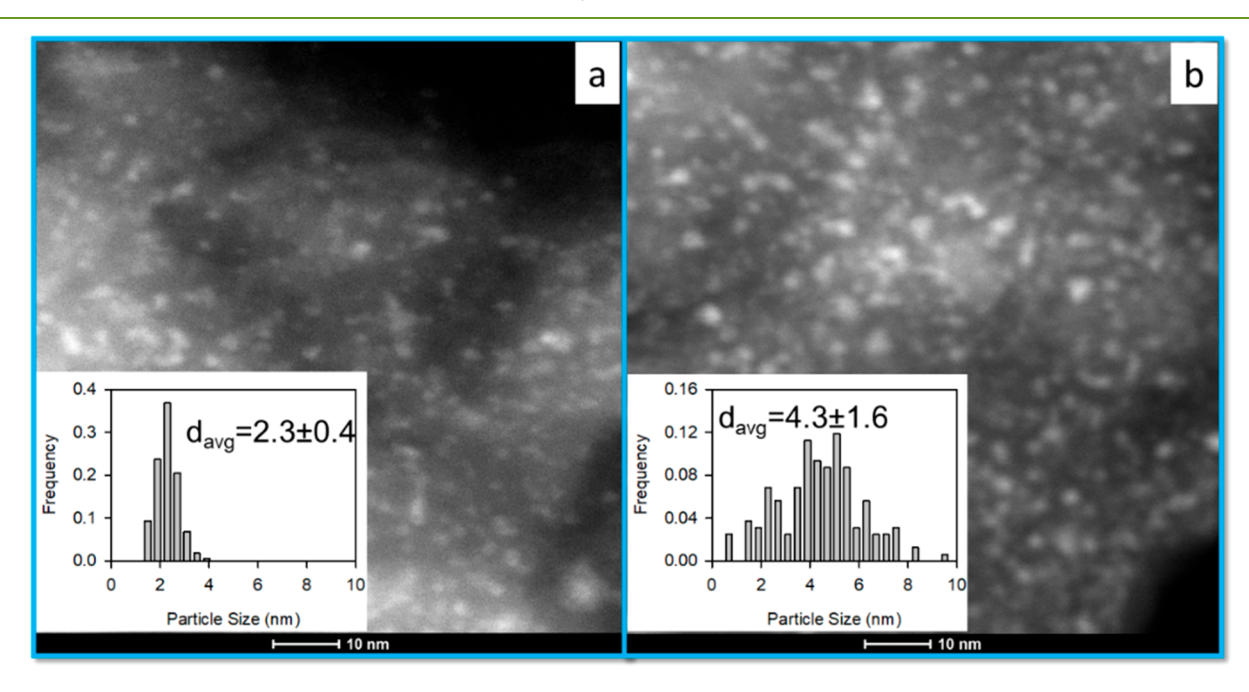


Figure 7. HAADF-STEM images of (a) fresh Ru/C and (b) Ru/C following the fourth reaction cycle in the catalyst reuse experiment depicted in Figure 6. Insets show Ru particle size distributions.

Table 2. Ru/C Catalyst Properties

	catalyst	BET surface area $(m^2 g^{-1})$	total pore volume ^{a} (cm ^{3} g ^{-1})	average pore diameter (nm)	metal loading (wt %)	metal dispersion (%)	Ru particle size—TEM (nm)
	fresh Ru/C	735.3	0.64	3.8	3.9	47	2.3 ± 0.4
1	used Ru/C after fourth	38.9	0.49	14.7	2.0	1.3	4.3 ± 1.6
	run						

^aAdsorption total pore volume at $P/P_0 = 0.97$. ^bCalculated from total pore volume and BET surface area.

the first reduction peak located at 65 °C and the second broad reduction peak above 400 °C. The reduction peak of supported Ru-oxides formed during catalyst calcination has been reported to vary between 65 and 185 °C. 39,40 Thus, the first peak observed here falls into this range, indicating partial oxidation of metallic Ru in the fresh Ru/C catalyst. The TPR profile for Ru/C after the fourth cycle was markedly different. A much lower intensity of first reduction peak indicated reduction of the Ru oxide coating (or dissolution) during the hydrothermal process, leaving a more metallic surface phase. A wide dip between 400 and 500 °C for the Ru/C used after the fourth run matches the in situ H2 production from the pyrolysis of residual fatty acid or its products. 41 Thus, the negative peak in TPR provides evidence to support the conclusion that some of the fatty acid or its products deposited within the pores or the surface of the spent catalyst. The second reduction peak is assigned to the direct reduction of aldehyde, quinone, and phenol groups on the carbon support.42

The reduction of Ru oxides to Ru metal during hydrothermal reactions was also supported by XPS analysis (Figure S9). The $Ru(3p_{3/2})$ binding energies were determined at 462.2 and 463.2 eV for the Ru metal and Ru-oxide in previous studies. 43 Figure S9 shows the major peak for fresh Ru/C was located at 463.2 eV, indicating the presence of Ru-oxide. However, following hydrothermal reaction, the $Ru(3p_{3/2})$ peak shifted to 462.2 eV, the same position as that observed with ex situ H₂ pretreated Ru/C, suggesting the used Ru/C was in a more reduced state. In sum, the deactivation of Ru/C likely resulted from a combination of factors, including (i) collapse of the support structure; (ii) blocking the micropores or covering the active sites by the reaction feedstock, products, or coking residues; (iii) leaching of Ru from the support; and (iv) sintering of Ru particles. These findings suggest the need for further studies to identify the factors controlling catalyst stability, deactivation, and regeneration, particularly when operated continuously in a fixed bed reactor configuration.

DISCUSSIONS AND IMPLICATIONS

In contrast with Pt/C, stearic acid conversion with Ru/C leads to the formation of a mixture of cracking products in addition to the DOX product n-heptadecane (C₁₇). The products with Ru/C include a series of hydrocarbons with a carbon number ranging from 7 to 17 (C_7-C_{17}) , which shifts to shorter chain alkanes with increasing reaction time and elevated H2 pressures in the reactor headspace. Some limited cracking may be ideal for tuning the fuel properties of the green diesel product to better match those of petroleum-derived diesel fuel (containing 10-15 carbon atoms) and jet fuels (contain 5-16 carbon atoms). Thus, we propose that the dual DOX + cracking activity coupled with the low cost of Ru/C may be ideal for hydrothermal green diesel production from lipid feedstocks. The presence of aromatic hydrocarbons in the petroleum diesel or the jet diesel leads to the incomplete combustion of fuel, and polycyclic aromatic hydrocarbons (PAHs) of a higher concentration result in higher emissions of these compounds by vehicle exhaust.³⁶ Thus, the green diesel obtained in this study has some advantages for the following reasons: (i) more complete combustion leading to the higher-usage of this green diesel than other diesels; (ii) chemically identical to the diesel made from petroleum, ^{29,44} with one significant difference—up to 85% lower greenhouse gas emissions vs diesel from petroleum based on UOP's lifecycle analysis; (iii) can be used in existing engines without any significant modification; 6,44 and (iv) prolonged engine lifetimes due to potentially fewer coking deposits. In addition, the head gas pressure has a significant influence on the conversion of feedstocks, but the exact mechanism is not clear enough, which deserves further study. Achieving the desired alkane mixture will require careful monitoring and control of the reaction environment, and further work is needed to understand the key factors controlling DOX and cracking reactions, ideally under continuous flow reaction conditions that are more consistent with industrially relevant reactor systems. A life cycle assessment and techno-economic evaluation (LCA/TEA), which includes an economic evaluation, energy balance, and environmental impacts, is also necessary in the future to better quantify the contributions from individual aspects of the conversion process, including the feedstock and the catalysts.

CONCLUSIONS

In summary, results from catalyst screening experiments identified Ru/C as a promising lower cost alternative to Pt/ C for hydrothermal processing of fatty acids and lipids in the absence of external H2 supplies. The reactivity of this catalyst was examined in detail, demonstrating complete conversion of stearic acid (model saturated fatty acid) and a triacylglyceride lipid, producing a range of liquid (C_7-C_{17}) and gas (C_1-C_5) alkane products. Conversion of the lipid was found to be much faster than stearic acid due to in situ H2 generation by aqueous phase reforming of the glycerol coproduct formed during the initial lipid hydrolysis step. Elevated reactor N2 pressure and H₂ pressure both accelerated stearic acid conversion reactions, suggesting there is room for further reactor optimization. Deactivation of the catalyst was observed over repeated reaction cycles, indicating the need to better understand and improve on-stream stability. An initial analysis of the contributing modes of deactivation suggests potential directions for improved material design or regeneration

ASSOCIATED CONTENT

S Supporting Information

The Supporting Information is available free of charge on the ACS Publications website at DOI: 10.1021/acssuschemeng.9b00215.

> Catalytic activity of the carbon support, Ru/C, and Ru/ Al₂O₃ (Figure S1); liquid product yields from stearic

acid vs heptadecane (Figure S2); alkane selectivity under N_2 (Figure S3); effect of N_2 pressure (Figure S4); influence of headspace gas and H_2 -producing amendments (Figure S5); products of glycerol (Figure S6); product selectivity under H_2 (Figure S7); TPR profiles (Figure S8); XPS (Figure S9); prices of catalysts (Table S1) (PDF)

AUTHOR INFORMATION

Corresponding Author

*E-mail: strthmnn@mines.edu.

ORCID ®

Jing Zhang: 0000-0002-7518-3388 Xiangchen Huo: 0000-0002-7932-4563 Yalin Li: 0000-0002-8863-4758

Notos

The authors declare no competing financial interest.

ACKNOWLEDGMENTS

This work was supported by the National Science Foundation (CBET-1804513), the NSF Engineering Research Center for Reinventing the Nation's Urban Water Infrastructure (Re-NUWIt; EEC-1028968), and the National Natural Science Foundation of China (51878095).

ACRONYMS

BE Binding energy

BET Brunauer-Emmett-Teller BJH Barrett-Joyner-Halenda

DOX Decarboxylation
FAMES Fatty acid methyl esters
FID Flame ionization detector

HAADF-STEM High-angle annular dark-field scanning-trans-

mission electron microscopy

HDO Hydrodeoxygenation

TCD Thermal conductivity detector TOF₀ Initial turnover frequency

TPR Temperature-programmed reduction XPS X-ray photoelectron spectroscopy

REFERENCES

- (1) Wang, F.; Jiang, J. C.; Wang, K.; Zhai, Q. L.; Sun, H.; Liu, P.; Feng, J. F.; Xia, H. H.; Ye, J.; Li, Z. X.; Li, F. L.; Xu, J. M. Activated carbon supported molybdenum and tungsten carbides for hydrotreatment of fatty acids into green diesel. *Fuel* **2018**, 228, 103–111.
- (2) Kordouli, E.; Pawelec, B.; Bourikas, K.; Kordulis, C.; Fierro, J. L. G.; Lycourghiotis, A. Hydrodeoxygenation of phenol on bifunctional Ni-based catalysts: Effects of Mo promotion and support. *Appl. Catal., B* **2018**, *229*, 139–154.
- (3) Putra, R.; Lestari, W. W.; Wibowo, F. R.; Susanto, B. H. Fe/Indonesian natural zeolite as hydrodeoxygenation catalyst in green diesel production from palm oil. *Bull. Chem. React. Eng. Catal.* **2018**, 13, 245–255.
- (4) Srifa, A.; Kaewmeesri, R.; Fang, C.; Itthibenchapong, V.; Faungnawakij, K. Roles of monometallic catalysts in hydrodeoxygenation of palm oil to green diesel. *Chem. Eng. J.* **2018**, *345*, 107–113.
- (5) Sousa, F. P.; Silva, L. N.; de Rezende, D. B.; de Oliveira, L. C. A.; Pasa, V. M. D. Simultaneous deoxygenation, cracking and isomerization of palm kernel oil and palm olein over beta zeolite to produce biogasoline, green diesel and biojet-fuel. *Fuel* **2018**, 223, 149–156.
- (6) Honeywell UOP Home Page. https://www.uop.com/ (accessed July 23, 2019).

- (7) Vardon, D. R.; Sharma, B. K.; Jaramillo, H.; Kim, D.; Choe, J. K.; Ciesielski, P. N.; Strathmann, T. J. Hydrothermal catalytic processing of saturated and unsaturated fatty acids to hydrocarbons with glycerol for in situ hydrogen production. *Green Chem.* **2014**, *16*, 1507–1520.
- (8) Sari, E. Green diesel production via catalytic hydrogenation/decarboxylation of triglycerides and fatty acids of vegetable oil and brown gease. Doctor of Philosophy, Wayne State University, 2013.
- (9) Santillan-Jimenez, E.; Crocker, M. Catalytic deoxygenation of fatty acids and their derivatives to hydrocarbon fuels via decarboxylation/decarbonylation. *J. Chem. Technol. Biotechnol.* **2012**, 87, 1041–1050.
- (10) Peng, B. X.; Zhao, C.; Kasakov, S.; Foraita, S.; Lercher, J. A. Manipulating catalytic pathways: Deoxygenation of palmitic acid on multifunctional catalysts. *Chem. Eur. J.* **2013**, *19*, 4732–4741.
- (11) Herskowitz, M.; Landau, M. V.; Reizner, Y.; Berger, D. A commercially-viable, one-step process for production of green diesel from soybean oil on Pt/SAPO-11. *Fuel* **2013**, *111*, 157–164.
- (12) Fu, J.; Lu, X. Y.; Savage, P. E. Hydrothermal decarboxylation and hydrogenation of fatty acids over Pt/C. *ChemSusChem* **2011**, *4*, 481–486.
- (13) Fu, J.; Lu, X. Y.; Savage, P. E. Catalytic hydrothermal deoxygenation of palmitic acid. *Energy Environ. Sci.* **2010**, *3*, 311–317.
- (14) Kim, D.; Vardon, D. R.; Murali, D.; Sharma, B. K.; Strathmann, T. J. Valorization of waste lipids through hydrothermal catalytic conversion to liquid hydrocarbon fuels with in situ hydrogen production. ACS Sustainable Chem. Eng. 2016, 4, 1775–1784.
- (15) Fu, J.; Shi, F.; Thompson, L. T.; Lu, X. Y.; Savage, P. E. Activated carbons for hydrothermal decarboxylation of fatty acids. *ACS Catal.* **2011**, *1*, 227–231.
- (16) Date, A. W. Analytic Combustion: With Thermodynamics, Chemical Kinetics and Mass Transfer, 1st ed.; Cambridge University Press. 2011.
- (17) Chevron Products Company. Aviation Fuels Technical Review, 2007. Chevron Corporation Home Page. https://www.chevron.com/(accessed July 23, 2019).
- (18) Catalysts Division of BASF Home Page. https://catalysts.basf.com/ (accessed Jan 10, 2019).
- (19) Snare, M.; Kubickova, I.; Maki-Arvela, P.; Eranen, K.; Murzin, D. Y. Heterogeneous catalytic deoxygenation of stearic acid for production of biodiesel. *Ind. Eng. Chem. Res.* **2006**, *45*, 5708–5715.
- (20) Miao, C.; Marin-Flores, O.; Dong, T.; Gao, D.; Wang, Y.; Garcia-Pérez, M.; Chen, S. Hydrothermal catalytic deoxygenation of fatty acid and bio-oil with in situ H₂. ACS Sustainable Chem. Eng. **2018**, *6*, 4521–4530.
- (21) Peng, G.; Vogel, F.; Refardt, D.; Ludwig, C. Catalytic supercritical water gasification: Continuous methanization of chlorella vulgaris. *Ind. Eng. Chem. Res.* **2017**, *56*, 6256–6265.
- (22) Peng, G.; Ludwig, C.; Vogel, F. Catalytic supercritical water gasification: Interaction of sulfur with ZnO and the ruthenium catalyst. *Appl. Catal., B* **2017**, 202, 262–268.
- (23) Hossain, M. Z.; Chowdhury, M. B.I.; Jhawar, A. K.; Xu, W. Z.; Charpentier, P. A. Continuous low pressure decarboxylation of fatty acids to fuel-range hydrocarbons with in situ hydrogen production. *Fuel* **2018**, *212*, 470–478.
- (24) Brown, T. M.; Duan, P. G.; Savage, P. E. Hydrothermal liquefaction and gasification of nannochloropsis sp. *Energy Fuels* **2010**, 24, 3639–3646.
- (25) Yeh, T. M.; Hockstad, R. L.; Linic, S.; Savage, P. E. Hydrothermal decarboxylation of unsaturated fatty acids over PtSnx/C catalysts. *Fuel* **2015**, *156*, 219–224.
- (26) Yeh, T. M.; Linic, S.; Savage, P. E. Deactivation of Pt Catalysts during Hydrothermal Decarboxylation of Butyric Acid. *ACS Sustainable Chem. Eng.* **2014**, *2*, 2399–2406.
- (27) Bhattacharjee, S.; Tan, C. S. Hydrodeoxygenation of oleic acid in hexane containing pressurized CO₂ using Fe/SBA-15 as catalyst. *J. Cleaner Prod.* **2017**, *156*, 203–213.
- (28) Hemminger, O.; Marteel, A.; Mason, M. R.; Davies, J. A.; Tadd, A. R.; Abraham, M. A. Hydroformylation of 1-hexene in supercritical

- carbon dioxide using a heterogeneous rhodium catalyst. 3. Evaluation of solvent effects. *Green Chem.* **2002**, *4*, 507–512.
- (29) Jessop, P. G.; Subramaniam, B. Gas-Expanded liquids. *Chem. Rev.* **2007**, *107*, 2666–2694.
- (30) Wei, H.-H.; Yen, C. H.; Lin, H.-W.; Tan, C.-S. Synthesis of bimetallic Pd Ag colloids in CO₂-expanded hexane and their application in partial hydrogenation of phenylacetylene. *J. Supercrit. Fluids* **2013**, *81*, 1–6.
- (31) Li, T.; Cheng, J.; Zhang, X.; Liu, J. F.; Huang, R.; Zhou, J. H. Jet range hydrocarbons converted from microalgal biodiesel over mesoporous zeolite-based catalysts. *Int. J. Hydrogen Energy* **2018**, *43*, 9988–9993.
- (32) Nakagawa, Y.; Oya, S.; Kanno, D.; Nakaji, Y.; Tamura, M.; Tomishige, K. Regioselectivity and reaction mechanism of Rucatalyzed hydrogenolysis of squalane and model alkanes. *ChemSusChem* **2017**, *10*, 189–198.
- (33) Yu, J. D.; Lu, X. Y.; Shi, Y. J.; Chen, Q. L.; Guan, Q. Q.; Ning, P.; Tian, S. L.; Gu, J. J. Catalytic gasification of lignite in supercritical water with Ru/CeO₂-ZrO₂. *Int. J. Hydrogen Energy* **2016**, *41*, 4579–4591.
- (34) Peng, G.; Ludwig, C.; Vogel, F. Ruthenium dispersion: A key parameter for the stability of supported ruthenium catalysts during catalytic supercritical water gasification. *ChemCatChem* **2016**, *8*, 139–141.
- (35) Guan, Q. Q.; Huang, X. D.; Liu, J.; Gu, J. J.; Miao, R. R.; Chen, Q. L.; Ning, P. Supercritical water gasification of phenol using a Ru/CeO₂ catalyst. *Chem. Eng. J.* **2016**, 283, 358–365.
- (36) Treusch, K.; Schwaiger, N.; Schlackl, K.; Nagl, R.; Rollett, A.; Schadler, M.; Hammerschlag, B.; Ausserleitner, J.; Huber, A.; Pucher, P.; Siebenhofer, M. High-throughput continuous hydrodeoxygenation of liquid phase pyrolysis oil. *Ract. Chem. Eng.* **2018**, *3*, 258–266.
- (37) Ping, E. W.; Pierson, J.; Wallace, R.; Miller, J. T.; Fuller, T. F.; Jones, C. W. On the nature of the deactivation of supported palladium nanoparticle catalysts in the decarboxylation of fatty acids. *Appl. Catal., A* **2011**, *396*, 85–90.
- (38) Bernas, H.; Eranen, K.; Simakova, I.; Leino, A. R.; Kordas, K.; Myllyoja, J.; Maki-Arvela, P.; Salmi, T.; Murzin, D. Y. Deoxygenation of dodecanoic acid under inert atmosphere. *Fuel* **2010**, *89*, 2033–2039
- (39) Hosokawa, S.; Kanai, H.; Utani, K.; Taniguchi, Y.; Saito, Y.; Imamura, S. State of Ru on CeO_2 and its catalytic activity in the wet oxidation of acetic acid. *Appl. Catal., B* **2003**, *45*, 181–187.
- (40) Deng, W. P.; Tan, X. S.; Fang, W. H.; Zhang, Q. H.; Wang, Y. Conversion of cellulose into sorbitol over carbon nanotube-supported ruthenium catalyst. *Catal. Lett.* **2009**, *133*, 167–174.
- (41) Youssef, E. A.; Nakhla, G.; Charpentier, P. A. Oleic acid gasification over supported metal catalysts in supercritical water: Hydrogen production and product distribution. *Int. J. Hydrogen Energy* **2011**, *36*, 4830–4842.
- (42) Kundu, S.; Wang, Y. M.; Xia, W.; Muhler, M. J. Thermal stability and reducibility of oxygen-containing functional groups on multiwalled carbon nanotube surfaces: A quantitative high-resolution XPS and TPD/TPR Study. *J. Phys. Chem. C* **2008**, *112*, 16869–16878.
- (43) NIST X-ray Photoelectron Spectroscopy Database Home Page. https://srdata.nist.gov/xps/Default.aspx (accessed July 23, 2019).
- (44) Othman, M. F.; Adam, A.; Najafi, G.; Mamat, R. Green fuel as alternative fuel for diesel engine: A review. *Renewable Sustainable Energy Rev.* **2017**, *80*, 694–709.